

Heliostat Wind Load Field Measurements at the University of Adelaide Atmospheric Boundary Layer Research Facility (ABLRF)

Matthew Marano¹[\[https://orcid.org/0000-0003-1519-3100\]](https://orcid.org/0000-0003-1519-3100), Matthew Emes²[\[https://orcid.org/0000-0003-4147-4387\]](https://orcid.org/0000-0003-4147-4387),
Azadeh Jafari³[\[https://orcid.org/0000-0003-1951-6106\]](https://orcid.org/0000-0003-1951-6106), and Maziar Arjomandi⁴[\[https://orcid.org/0000-0002-7669-2221\]](https://orcid.org/0000-0002-7669-2221)

¹ PhD Candidate, Centre for Energy Technology, School of Mechanical Engineering, University of Adelaide, Adelaide, SA 5005, Australia. Email: matthew.marano@adelaide.edu.au

² Postdoctoral Research Fellow, Australia

³ Postdoctoral Research Fellow, Australia

⁴ Professor, Australia

Abstract. The University of Adelaide has recently commissioned a facility dedicated to investigating the atmospheric boundary layer (ABL) for the analysis of wind loads on full-scale heliostats. Wind tunnel testing is an affordable way to analyse loads on a scaled structure before committing to a full-scale design. Scale testing however has its challenges as most cases in literature fail to correctly scale the ABL when scaling a model due to the differences between the ratio of the heliostat chord to the boundary layer depth in a wind tunnel and ABL. There is a lack of direct comparison between wind tunnel and full-scale heliostat wind loads. The Atmospheric Boundary Layer Research Facility (ABLRF) consists of arrays of ultrasonic anemometers and a 1.5 aspect ratio heliostat, mounted on a 6-axis load cell, for the comparison of loads measured in the wind tunnel with a full-scale model. Preliminary results categorise the site to have a roughness of 0.01 m to 0.03 m indicating open country farmland, when compared to standards. Comparison between coefficients of lift force, drag force, and hinge moment on the heliostat model at a single elevation angle at the ABLRF and wind tunnel models in literature verify the commissioning of the site, allowing for further in-depth analysis of wind load coefficients at varying elevation and azimuth angles.

Keywords: Atmospheric Boundary Layer, Field Measurements, Aerodynamic Coefficients, Lift Force, Drag Force, Integral Length Scale, Surface Roughness, Wind Loads, Turbulence

1. Introduction

With an ever-increasing need for clean energy production, the need to reduce the cost of renewable energy resources becomes more critical. The Paris agreement, signed by 196 countries aims to reduce greenhouse gas emissions for a carbon neutral world to be realised by 2050 [1]. Concentrated solar power (CSP) has demonstrated potential to contribute to power production and heavy industry decarbonisation through production of green process heat. But cost and efficiency, in terms of operating conditions, need to be improved for the technology to be more readily implemented.

A significant cost component of a CSP power tower plant is associated with the cost of the heliostats, making up to 34% of the total cost of a plant [2]. This cost can be reduced by optimising heliostat design and efficiency through prolonging operating conditions. For example, designing for operation at higher wind loads can result in increasing the operating

time of the field before being necessary to stop the production of energy by stowing the heliostats [3]. In addition, overestimation of wind loads, such as stow wind loads identified as being overestimated in a number of heliostat studies, result in a greater heliostat material cost [4,5]. Wind loads also affect the operating efficiency of the plant through wind load induced vibrations, leading to beam misalignment [6], which can also be minimised through thoughtful heliostat design from a deeper understanding of wind loads.

Heliostat design can be optimised through scale testing in a wind tunnel (such as the work at The University of Adelaide) [7]. To conduct a proper wind tunnel simulation of the loads experienced by a heliostat in the atmospheric boundary layer (ABL) both the heliostat and ABL need to be scaled accordingly. Jafari et al. [8] highlighted this mismatch in boundary layer scaling with heliostats for wind tunnel analysis. A full-scale heliostat study that accurately accounts for atmospheric turbulence further improves the understanding of heliostat wind loads and hence support the reduction of the cost of energy production by a heliostat field.

As part of the Australian Solar Thermal Research Institute (ASTRI) heliostat project, the University of Adelaide has set up the Atmospheric Boundary Layer Research Facility (ABLRF) to investigate the accuracy of wind tunnel testing for heliostat structures. The ABLRF consists of an array of ultrasonic anemometers for the measurement of three-dimensional wind speed, turbulence intensities, and length scales, and an instrumented heliostat equipped with pressure sensors and a 6-axis load cell to analyse the wind loads due to a turbulent flow field in outdoor conditions.

2. Method

Figure 1(a) shows a schematic of the Atmospheric Boundary Layer Research Facility (ABLRF). It consists of an array of fourteen 81005A RM Young three-dimensional ultrasonic anemometers longitudinally, laterally, and vertically arranged to capture three-dimensional wind speed, temperature, and speed of sound at 32 Hz, for an afternoon north-easterly wind. This is the prevailing wind direction for high wind speeds above 10 m/s based on Bureau of Meteorology (BoM) weather station 023122 cup anemometer observations from 2013-2019 [9], as shown in Figure 1(b). Five of the ultrasonic anemometers are logarithmically positioned along the height of a 12 m lattice tower (1.6 m, 3.1 m, 4.6 m, 7.9 m, and 12 m), which allows for the ABL to be properly characterised. Lateral to the prevailing wind direction are another five sensors positioned at 3 metre intervals atop 3 metre masts. The remaining four are positioned longitudinally to the prevailing wind, upstream from a heliostat (Figure 1a), at 5 metre intervals at a height of 3 metres. The mean wind speeds are verified with the use of a series of cup anemometers, labelled in Figure 2.

The heliostat has an aspect ratio of 1.5 (3 m width x 2 m height) with a hinge height of 1.6 m. A 6-axis 10 kN/1 kNm load cell (K6d175) is located below the hinge to measure wind loads on the heliostat (Figure 3). Two 3 kg linear actuators, allow for investigation of various elevation (α) and azimuth (β_H) angles, 0-90° and $\pm 45^\circ$ from west, respectively. The heliostat also contains 48 Honeywell HSC series ± 600 Pa differential pressure sensors connected to corresponding ports distributed over its upper and lower surfaces. The ultrasonic anemometers and load cell collect data at 32 Hz and 500 Hz, respectively. An on-site computer is used to continuously log the data. The site is powered by a pair of 315 W photovoltaic panels and four 102 Ah batteries.

The heliostat on the 24th May 2022 had an elevation angle (α) of 10° and an azimuth angle (β_H) of 1.5°, in relation to west, see Figure 3. The heliostat azimuth angle (β_H) was adjusted in calculations to model the lift and drag in relation to the changing wind flow direction (ϕ) using Equation 1 for north-easterly wind:

$$\beta_w(t) = \beta_H + \phi(t) + 90^\circ \quad (1)$$

Load cell coordinates are transformed to the heliostat coordinate system, the resulting drag force is the magnitude of the x and y force components. Positive lift is expected as the flow is approaching from the back of the heliostat. The coefficients of drag, lift, and hinge moment were calculated from Equations 2 and 3 respectively:

$$C_{Fx} = F_x / \left(\frac{1}{2} \rho U^2 A \right), C_{Fz} = F_z / \left(\frac{1}{2} \rho U^2 A \right) \quad (2)$$

$$C_{MHy} = M_{Hy} / \left(\frac{1}{2} \rho U^2 A c \right) \quad (3)$$

The collected data has an accuracy of ± 0.05 m/s, $\pm 2^\circ$, and $\pm 2^\circ$ C, with a resolution of 0.01 m/s, 0.1° , and 0.01° C, for wind velocity, direction, and temperature, respectively. The heliostat angles have an accuracy of $\pm 0.5^\circ$. The load offsets for calibration of the load cell were taken in stow position at a wind velocity of less than 0.35 m/s.

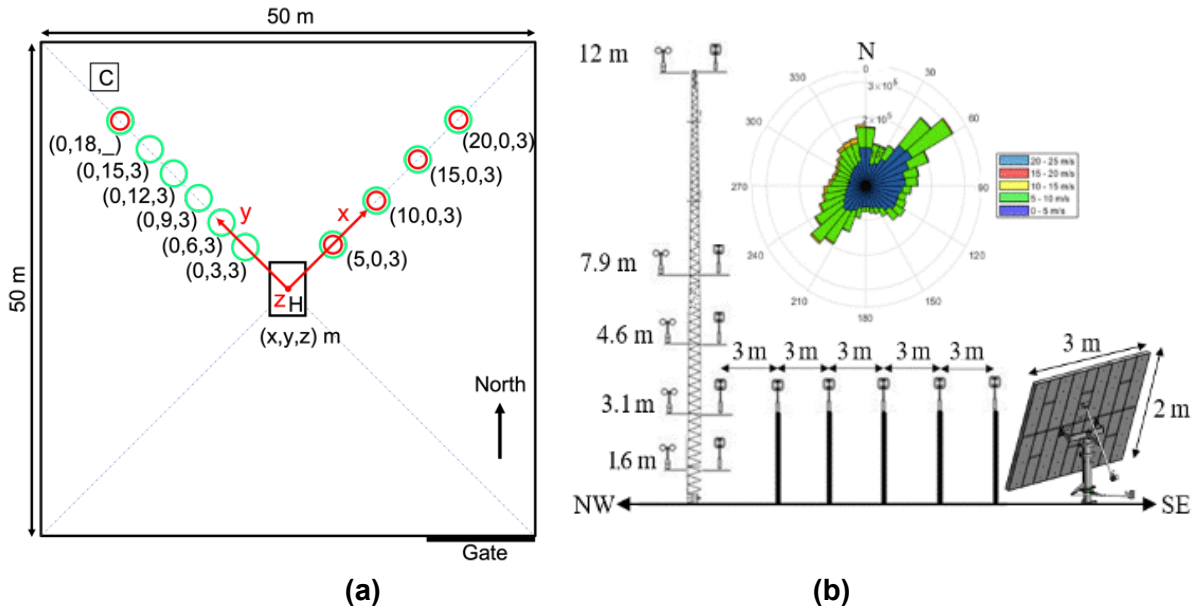


Figure 1. (a) A top view schematic of the Atmospheric Boundary Layer Research Facility (ABLRF) indicating the positioning of the sensors within the fenced site. (b) The layout of the ABLRF indicating the heights and spacings of the ultrasonic anemometers with an inset wind rose recorded from the Bureau of Meteorology weather station 023122 [9] cup anemometer indicating a north-easterly prevailing wind at the site.



Figure 2. Image of the ABLRF looking north with the installed Ultrasonic Anemometers (UA), Cup Anemometers (CA), and Load Cell (LC) configuration labelled.

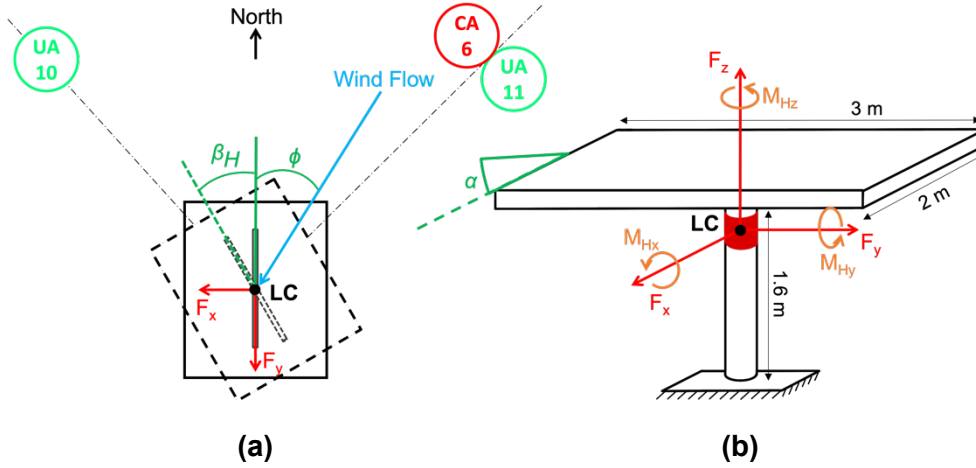


Figure 3. (a) A top view schematic diagram of heliostat load cell axes. (b) A side view schematic diagram of heliostat load cell axes.

3. Results

Figure 4 shows the 10-minute averaged time series on the afternoon of 24th May 2022, for UA1-5 (Figure 2). The flow direction in Figure 4(a) is calculated by finding the angle between the u and v components of wind velocity where u and v are the easterly and northerly horizontal velocity components, respectively, indicating the prevailing north-easterly wind direction. Unstable convective conditions are identified as characterised by the Monin-Obukhov stability parameter z/L [10]:

$$z/L = g/\theta_0 \times (\overline{kzw'\theta'}) / -u_\tau^3 \quad (4)$$

where $k = 0.41$ is von Karman's constant, $u_\tau = ((u'w')^2 + (v'w')^2)^{1/4}$ (m/s) [11] is friction velocity, z (m) is the height above the ground, $g = 9.81 \text{ m/s}^2$ is gravitational acceleration, w' (m/s) is the vertical component of the fluctuating wind velocity, θ_0 (K) is the mean temperature, and $\overline{w'\theta'}$ ($\text{m/s}^2 \text{ K}$) is the surface heat flux. The stability parameter $z/L < 0$ throughout the afternoon when temperatures are high, as mixing is occurring between the different layers of the boundary layer due to convective currents from a warmer surface. The stability parameter then approaches a stable condition ($z/L > 0$) as sunset approaches. This relates to the decrease in temperature in Figure 4(c) and a rapid reduction in wind velocity in Figure 4(b) from 15:45, as convective forces decrease with the decline in surface temperature, and a stable boundary layer forms into the evening.

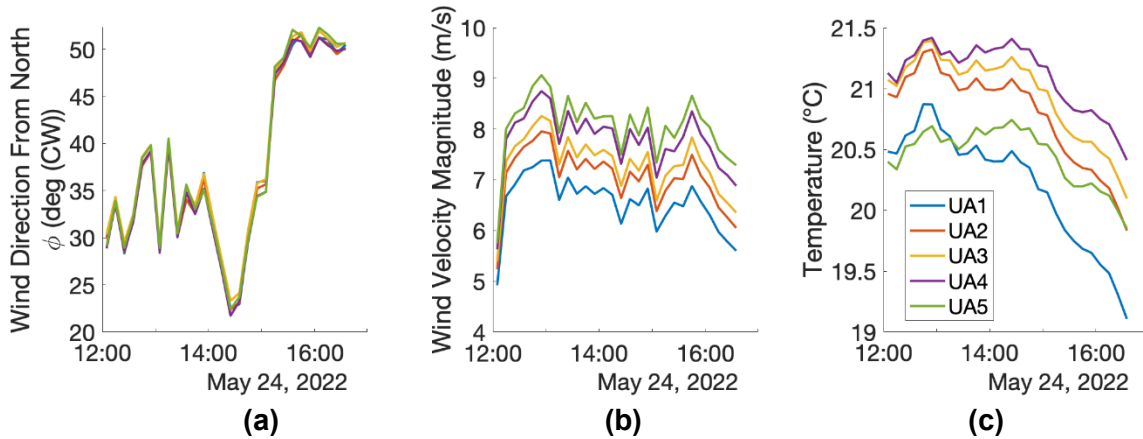


Figure 4. (a) 10-minute averages of time series for each ultrasonic sensor over the height of the lattice tower during the time period with a prevailing north-easterly wind direction. (b) The wind velocity magnitude of horizontal wind components reaches a peak at 13:00 and begins

to settle from 15:45. (c) The temperature along the height of the lattice tower decreases in the late afternoon, causing the decrease in wind velocity.

The boundary layer profile is plotted along the 12 m height of the lattice tower, averaged over a 10-minute period at 14:14 on 24th May 2022 in Figure 5(a). The mean velocity profile is consistent with a log law profile [12]:

$$U(z) = u_\tau / k \times \ln(z) + A \quad (5)$$

where $A = 6.5$ and $u_\tau = 0.3$ m/s at the lowest measurement height of 1.6 m. The boundary layer height calculated at 99% freestream velocity of the fitted log law profile to the 12 m tower ABLRF measurements is calculated to be 1.67 km, which gives a similar value to calculating the minimum point for the gradient of velocity profile [13]. Analysing the same point in time but assuming neutral conditions, the depth is calculated as $cu_\tau/f = 726$ m with empirical constant $c = 0.2$, friction velocity $u_\tau = 0.3$ m/s and Coriolis force $f = 8.263 \times 10^{-5}$ rad/s at a latitude (-34.513259°) of the ABLRF [14]. The Ekman layer depth is calculated as $2ck\pi^2(u_\tau/f) = 2.94$ km for a neutral boundary layer [11,15]. Therefore, the average boundary layer depth is approximated as 1.353 km. A more accurate boundary layer depth can be obtained with velocity measurements taken at a greater height [13].

Figure 5(b) plots the longitudinal and vertical turbulence intensity components, Equation 6, against the $\pm 10\%$ uncertainty ESDU 85020 [16] profiles for the ABL with surface roughness heights of $z_0 = 0.01$ m and $z_0 = 0.03$ m. This indicates that the ABLRF site is representative of flat, open country terrain, and typical farmland, which is an accurate description of the site. The longitudinal turbulence intensity (I_u) is 18%, which is similar to ABL modelled in wind tunnel experiments [17,18,19].

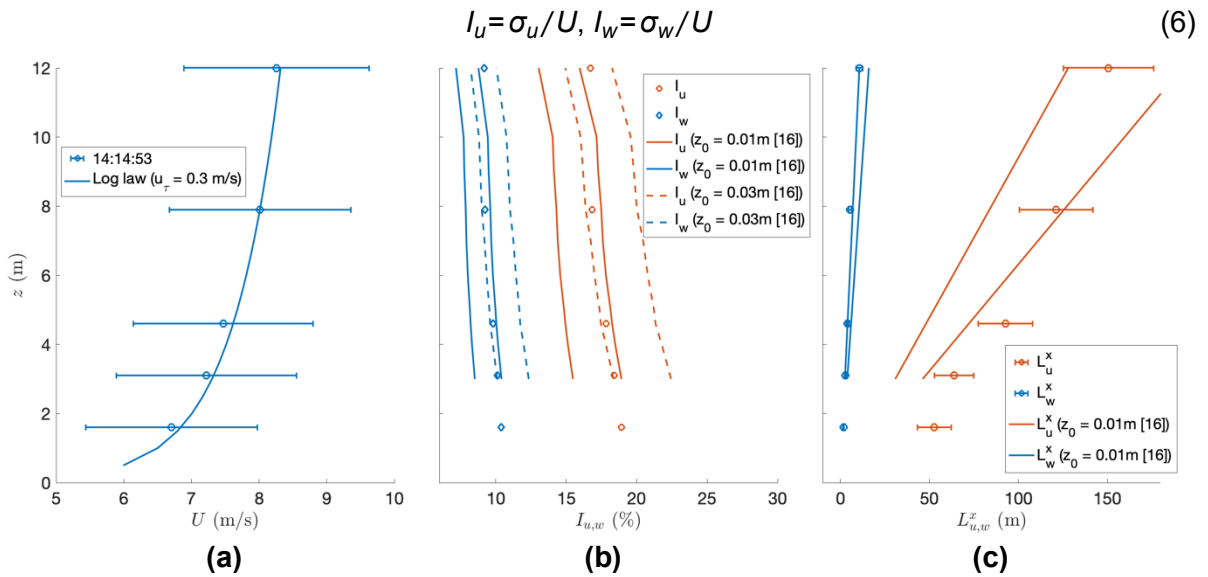


Figure 5. (a) Boundary layer velocity profile measured from sensors UA1-UA5 located on the 12 m lattice tower with a log law plot indicating a logarithmic profile with a friction velocity of 0.3 m/s. (b) The turbulence intensity also over the height of the 12 m lattice tower is plotted against ESDU 85020 [16] roughness profiles of $z_0 = 0.01$ m and $z_0 = 0.03$ m indicating the ABLRF has characteristics of flat, open country terrain, and typical farmland. Plots (a-b) are in reference to a 10-minute time period at 14:14 on the 24th May 2022. (c) ABLRF integral length scales over an unstable period plotted against the $\pm 20\%$ uncertainty ESDU 85020 [16] neutral boundary layer data in the longitudinal (L_u^x) and vertical (L_w^x) direction for a roughness value of $z_0 = 0.01$ m on 24th May 2022 from 13:40 – 14:50. As the measured vertical component is at the lower range, the vertical turbulence is shorter than predicted from the ESDU 85020 [16] data, but longer in the horizontal component at lower heights.

The integral length scale calculated from Equation 7 shows the average size of energy-containing turbulent eddies at a given height and flow direction [10]:

$$L_i^x = T_i^x(z)U(z) \quad (7)$$

where T_i^x (s) is the integral time scale of the fluctuating velocity component ($i = u, w$). Figure 5(c) shows the calculated length scales against the $\pm 20\%$ uncertainty ESDU 85020 [16] profiles over a 70-minute period from 13:40 to 14:50 on the 24th May 2022. The ABL is unsteady and varying during this period with an average $z/L = -0.79$, calculated using Equation 4. As ESDU 85020 [16] models a neutral boundary layer, this shows that the size of the vertical turbulence (L_w^x) is at the lower bound of the ESDU 85020 [16] data. Nevertheless, longitudinal components follow the upper bound of the ESDU 85020 [16] profile, showing the eddies are elongated in the longitudinal direction compared to neutrally stratified conditions, for a site roughness of $z_0 = 0.01$ m, further confirming the estimated roughness of the ABLRF from Figure 5(b).

Figure 6 plots the time series of 10-minute averaged values of the coefficients of drag force, lift force, and hinge moment, showing the variations in the loads due to the varying wind velocity, with the time 14:14 highlighted. The wind incident angle (β_w) at 14:14 is 122° with a turbulence intensity of 18%. The negative hinge moment is most likely due to there being a greater pressure near the leading edge of the heliostat [20]. Analysis of the installed pressure sensors will confirm this, as it could be linked to the vertical wind flow in the ABL. It should be noted that the ABLRF heliostat has a smooth backing surface, which will promote a reduction in drag forces.

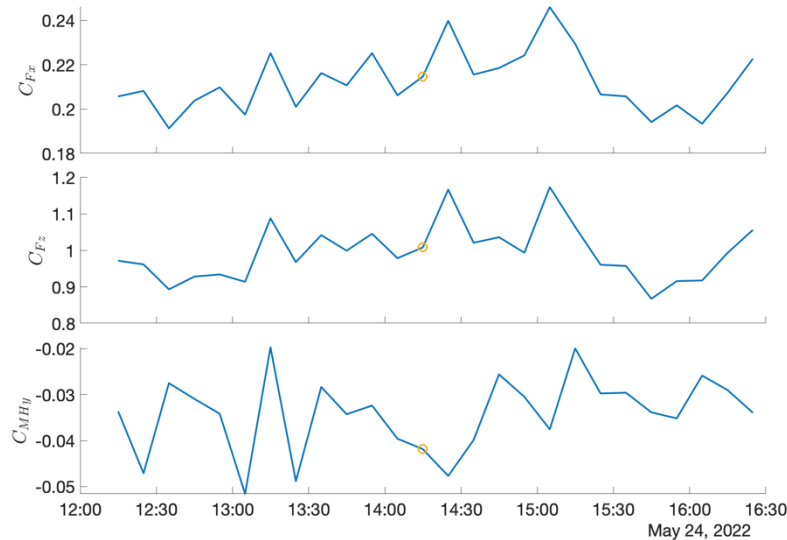


Figure 6. Time series of the coefficients of drag force, lift force, and hinge moment, showing the change in coefficient values with a change in flow velocity for $\alpha = 10^\circ$ and $\beta_w = 122^\circ$. The investigated time is highlighted at 14:14 for a turbulence intensity of 18%, $L_u^x = 52$ m, and $L_w^x = 1.76$ m at hinge height ($H = 1.6$ m).

4. Conclusion

The commissioning of the ABLRF at The University of Adelaide allows for the comparison and verification of wind tunnel experimentation of heliostats and modelling of the ABL. This study highlighted the layout of the ABLRF with the available sensors and recordings to be further investigated. Primary analysis of mean wind velocity and turbulence intensities verified the ABLRF has a roughness height between 0.01 m and 0.03 m, categorising the site as typical farmland with open country terrain during unstable boundary layer conditions, with small variations compared with ESDU 85020 [16]. The integral length scales were analysed

during an afternoon time period with reduced vertical length scales and increased longitudinal length scales at lower heights compared with ESDU 85020 [16] data for a neutral ABL with surface roughness of $z_0 = 0.01$ m, further confirming the estimated surface roughness of the ABLRF site. The coefficients of drag force, lift force, and hinge moment at the ABLRF allow for further investigation and comparison between full-scale and wind tunnel heliostat model load coefficients for additional operating angles, atmospheric boundary layer conditions and gust events.

Data availability statement

Data in the article can be accessed by contacting the authors.

Author contributions

Matthew Marano contributed to data curation, formal analysis, investigation, methodology, software, visualization, and writing (original draft). Matthew Emes contributed to conceptualization, data curation, investigation, methodology, supervision, validation, and writing (review). Azadeh Jafari contributed to conceptualization, supervision, validation, and writing (review). Maziar Arjomandi contributed to conceptualization, supervision, validation, and writing (review).

Competing interests

The authors declare no competing interests.

Funding

The work is funded by the Australian Renewable Energy Agency (ARENA) Grant 1-SRI002 as part of the Australian Solar Thermal Research Institute (ASTRI) P11 project.

Acknowledgement

The authors would like to acknowledge the contributions by Science and Engineering Technology Faculty Electronics and Instrumentation Team Leader Philip Schmidt to the field site preparation, mechanical and electrical installation, instrumentation commissioning and testing. The authors also acknowledge the contributions by Michael Rae and Mike Collins from CSIRO to the control panel and heliostat construction and commissioning. The project team would like to acknowledge the Centre for Energy Technology (CET), Institute for Sustainability, Energy and Resources (ISER) and the University of Adelaide Infrastructure Campus Estate manager, project manager, and Roseworthy farm manager for their support. Along with Warwick Grace from Conditions Over the Landscape (COtL) for donating three ultrasonic anemometers and four tripod masts in the longitudinal array. The work is funded by the Australian Solar Thermal Research Institute (ASTRI) heliostat project.

References

1. United Nations Climate Change, "Paris Agreement", United Nations Framework Convention on Climate Change, <https://unfccc.int/process-and-meetings/the-paris-agreement/the-paris-agreement> (last accessed 2 September 2022).
2. A. Pfahl, J. Coventry, M. Röger, F. Wolfertstetter, J. F. Vásquez-Arango, F. Gross, M. Arjomandi, P. Schwarzbözl, M. Geiger & P. Liedke, "Progress in heliostat development", *Solar Energy*, vol.152, pp.3-37, March, 2017, doi: <https://doi.org/10.1016/j.solener.2017.03.029>.
3. M. Emes, A. Jafari, M. collins, S. Wilbert, L. Zarzalejo, S, Siegrist & M. Arjomandi, "Stowing strategy for a heliostat field based on wind speed and direction", *AIP Conference Proceedings*, vol.2445, 120011, May, 2022, doi: <https://doi.org/10.1063/5.0085677>.

4. J. Coventry, J. Campbell, Y. Peng Xue, C. Hall, J. Kim, J. Pye, G. Burgess, D. Lewis, G. Nathan, M. Arjomandi, W. Stein, M. Blanco, J. Barry, M. Doolan, W. Lipinski & A. Beath, "HelioStat Cost Down Scoping Study", Australian Solar Thermal Research Initiative, 2016.
5. M. Emes, A. Jafari, A. Pfahl, J. Coventry, M. Arjomandi, "A review of static and dynamic heliostat wind loads", *Solar Energy*, vol.225, pp.60-82, Sept., 2021, doi: <https://doi.org/10.1016/j.solener.2021.07.014>.
6. M. J. Emes, A. Jafari, J. Coventry & M. Arjomandi, "The influence of atmospheric boundary layer turbulence on the design wind loads and cost of heliostats", *Solar Energy*, vol.207, pp.796-812, Sept, 2020, doi: <https://doi.org/10.1016/j.solener.2020.07.022>.
7. M. Arjomandi, M. Emes, A. Jafari, J. Yu, F. Ghanadi, R. Kelso, B. Cazzolato, J. Coventry & M. Collins, "A summary of experimental studies on heliostat wind loads in a turbulent atmospheric boundary layer", *AIP Conference Proceedings*, vol.2303, 030003, Dec., 2020, doi: <https://doi.org/10.1063/5.0028676>.
8. A. Jafari, F. Ghanadi, M. J. Emes, M. Arjomandi & B. S. Cazzolato, "Measurement of unsteady wind loads in a wind tunnel: Scaling of turbulence spectra", *Journal of Wind Engineering and Industrial Aerodynamics*, vol.193, July, 2019, doi: <https://doi.org/10.1016/j.jweia.2019.103955>.
9. Bureau of Meteorology, 2014, Data Services, <http://www.bom.gov.au/climate/data-services/> (last accessed 29.08.20).
10. M. J. Emes, M. Arjomandi, R. M. Kelso & F. Ghanadi, "Turbulence length scales in a low-roughness near-neutral atmospheric surface layer", *Journal of Fluid Mechanics*, Oct, 2019, doi: <https://doi.org/10.1080/14685248.2019.1677908>.
11. R. B. Stull, "An introduction to boundary layer meteorology", Kluwer Academic, 1988.
12. I. Marusic, J. P. Monty, M. Hultmark & A. J. Smits, "On the logarithmic region in wall turbulence", *Journal of Fluid Mechanics*, vol.716, R3, 2013, doi: <https://doi.org/10.1017/jfm.2012.511>.
13. M. Metzger, B. J. McKeon & H. Homes, "The near-neutral atmospheric surface layer: turbulence and non-stationarity", *Phil. Trans. R. Soc. A*, vol.365, pp 859-876, March, 2007, doi: <http://doi.org/10.1098/rsta.2006.1946>
14. A. P. van Ulden & A. A. M. Holtslag, "Estimation of Atmospheric Boundary Layer Parameters for Diffusion Applications", *Journal of Climate and Applied Meteorology*, vol.24, pp.1196-1207, Nov., 1985, doi: [http://doi.org/10.1175/1520-0450\(1985\)024<1196:EOABLP>2.0.CO;2](http://doi.org/10.1175/1520-0450(1985)024<1196:EOABLP>2.0.CO;2)
15. M. J. Emes, M. Arjomandi, R. M. Kelso & F. Ghanadi, "Turbulence length scales in a low-roughness near-neutral atmospheric surface layer", *Journal of Fluid Mechanics*, Oct, 2019, doi: <https://doi.org/10.1080/14685248.2019.1677908>.
16. ESDU 85020, 1985, "Characteristics of atmospheric turbulence near the ground - Part II: single point data for strong winds (neutral atmosphere)", Engineering Sciences Data Unit, London, UK.
17. A. Pfahl, M. Buselmeier & M. Zashke, "Wind loads on heliostats and photovoltaic trackers of various aspect ratios", *Solar Energy*, vol.85, no.9, pp.2185-2201, Sept, 2011, doi: <https://doi.org/10.1016/j.solener.2011.06.006>.
18. J. A. Peterka, Z. Tan, B. Bienkiewicz & J. E. Cermak, "Mean and Peak Wind Load Reduction on Heliostats", United States, 1987, doi: <https://doi.org/10.2172/6048728>.
19. M. Emes, A. Jafari, F. Ghanadi & M. Arjomandi, "Hinge and overturning moments due to unsteady heliostat pressure distributions in a turbulent atmospheric boundary layer", *Solar energy*, vol.192, pp.604-617, Nov., 2019, doi: <https://doi.org/10.1016/j.solener.2019.09.097>.
20. A. Jafari, M. Emes, B. Cazzolato, F. Ghanadi & M. Arjomandi, "An experimental investigation of unsteady pressure distribution on tandem heliostats", *AIP Conference Proceedings*, vol.2303, 030022, Dec, 2020, doi: <https://doi.org/10.1063/5.0028678>.